Mechanisms of endothelial cell dysfunction in cystic fibrosis

CrossMark

Licia Totani[a], Roberto Plebani[b,c], Antonio Piccoli[a], Sara Di Silvestre[b,c], Paola Lanuti[c,d],
Antonio Recchiuti[b,c], Eleonora Cianci[b,c], Giuseppe Dell'Elba[a], Silvio Sacchetti[e], Sara Patruno[b,c],
Simone Guarnieri[c,f], Maria A. Mariggiò[c,f], Veronica C. Mari[b,c], Marco Anile[g], Federico Venuta[g],
Paola Del Porto[h], Paolo Moretti[i], Marco Prioletta[b], Felice Mucilli[b], Marco Marchisio[c,d],
Assunta Pandolfi[b,c], Virgilio Evangelista[a], Mario Romano[b,c,*]

[a] Laboratory of Vascular Biology and Pharmacology, Fondazione Mario Negri Sud, Santa Maria Imbaro (CH), Italy
[b] Department of Medical, Oral and Biotechnological Sciences, G. D'Annunzio University, Chieti-Pescara, Italy
[c] Center on Aging Sciences and Translational Medicine (CeSI-MeT), G. D'Annunzio University, Chieti-Pescara, Italy
[d] Department of Medicine and Aging Sciences, G. D'Annunzio University, Chieti-Pescara, Italy
[e] Center for Synaptic Neuroscience, Italian Institute of Technology, Genoa, Italy
[f] Department of Neurosciences, Imaging and Clinical Sciences, G. D'Annunzio University, Chieti-Pescara, Italy
[g] Department of Thoracic Surgery, University of Rome "Sapienza", Rome, Italy
[h] Department of Biology and Biotechnology "Charles Darwin", Sapienza University, Rome, Italy
[i] Cystic Fibrosis Center, S. Liberatore Hospital, Atri, TE, Italy

ARTICLE INFO

ABSTRACT

Although cystic fibrosis (CF) patients exhibit signs of endothelial perturbation, the functions of the cystic fibrosis conductance regulator (CFTR) in vascular endothelial cells (EC) are poorly defined. We sought to uncover biological activities of endothelial CFTR, relevant for vascular homeostasis and inflammation. We examined cells from human umbilical cords (HUVEC) and pulmonary artery isolated from non-cystic fibrosis (PAEC) and CF human lungs (CF-PAEC), under static conditions or physiological shear. CFTR activity, clearly detected in HUVEC and PAEC, was markedly reduced in CF-PAEC. CFTR blockade increased endothelial permeability to macromolecules and reduced trans-endothelial electrical resistance (TEER). Consistent with this, CF-PAEC displayed lower TEER compared to PAEC. Under shear, CFTR blockade reduced VE-cadherin and p120 catenin membrane expression and triggered the formation of paxillin- and vinculin-enriched membrane blebs that evolved in shrinking of the cell body and disruption of cell-cell contacts. These changes were accompanied by enhanced release of microvesicles, which displayed reduced capability to stimulate proliferation in recipient EC. CFTR blockade also suppressed insulin-induced NO generation by EC, likely by inhibiting eNOS and AKT phosphorylation, whereas it enhanced IL-8 release. Remarkably, phosphodiesterase inhibitors in combination with a β_2 adrenergic receptor agonist corrected functional and morphological changes triggered by CFTR dysfunction in EC. Our results uncover regulatory functions of CFTR in EC, suggesting a physiological role of CFTR in the maintenance EC homeostasis and its involvement in pathogenetic aspects of CF. Moreover, our findings open avenues for novel pharmacology to control endothelial dysfunction and its consequences in CF.

1. Introduction

Cystic fibrosis (CF) is a genetic disease, caused by mutations in the cystic fibrosis transmembrane conductance regulator (CFTR) gene [1]. The CFTR protein regulates Cl^- and $HCO3^-$ secretion in ciliated and serous cells of submucosal glands and ducts, and in epithelial cells [2,3]. In the airways, CFTR dysfunction reduces the periciliary fluid volume and impairs the mucociliary clearance, promoting infection, inflammation and respiratory insufficiency [4]. CFTR dysfunction in cells deputed to the immune-surveillance and host response can contribute to CF pathogenesis [5–7].

The vascular endothelium is pivotal for the regulation of vascular

homeostasis and of the inflammatory response. It forms a semi-permeable barrier between tissues and the bloodstream, thereby regulating solute transport and immune cells trafficking. The endothelial barrier function is tightly controlled by intercellular adherence junctions (AJ) and tight junctions, interconnected with cytoskeletal proteins [8]. The transmembrane protein Vascular Endothelial cadherin (VE-cadherin) is the major structural component of endothelial AJ. p120-catenin protects VE-cadherin from being internalized and is required for the proper assembly of AJ and the maintenance of barrier function [9]. Endothelial cells (EC) are also engaged in transcellular exchanges by releasing either soluble mediators, including nitric oxide (NO) and interleukin (IL)-8 that control vascular tone and leukocyte recruitment, or microvesicles (EMV) that carry a repertoire of proteins, lipids and nucleic acids [10].

Despite its preeminent role in vasoregulation and inflammation, the vascular endothelium has been insufficiently investigated in CF. CFTR expression in EC and the involvement of CFTR in endothelial responses to hypoxia have been reported [11,12]. We and others documented that CF patients present peripheral biochemical signs of endothelial perturbation [13,14]. Moreover, microvascular dysfunction in CF patients has been recently reported [15]. Together with enhanced oxidant stress, unresolved inflammation and the extension of life expectancy, endothelial dysfunction could contribute to increase the cardiovascular risk for CF patients.

In the present report, we investigated the impact of CFTR loss-of-function on EC activities potentially related to cardiovascular risk and lung inflammation.

2. Materials and methods

DMEM and 199 media, fetal calf serum (FCS), penicillin and streptomycin were from Gibco (Waltham, Massachusetts, U.S.A.). HEPES was from Merk (Darmstadt, Germany). CFTRinh-172, formoterol fumarate and anti-p120 catenin antibody were from Santa Cruz Biotechnology (Dallas, Texas, U.S.A.). IL-1β (human, recombinant) was from Enzo Life Sciences (NY, USA). Roflumilast N-Oxide (RNO), the active metabolite of roflumilast was generously provided by Nycomed (Konstanz, Germany). Rolipram, Formoterol and Cilostamide were from Calbiochem (Vimodrone, Milano, Italy). Anti-VE-Cadherin antibody and DRAQ5 were from Abcam (Cambridge, U.K.). Anti-paxillin and anti-vinculin antibodies were from BD (BD Trasduction Laboratories, Milano Italy) and Sigma-Aldrich (St Louis, MO, USA), respectively. Phalloidin-TRITC and fluorescein isothiocyanate (FITC)-conjugated dextran (FD4; 3-5kDA) were from Sigma (Saint Louis, MO, U.S.A.).

2.1. Cells

Human umbilical vein endothelial cells (HUVEC) were isolated as previously described [16] and cultured in DMEM/199 medium (50% volume), endothelial cell growth supplement (100 μg/mL), heparin (15 U/mL) penicillin-streptomycin (100 μg/mL, each) and FCS (12%) at 37 °C under 5% CO_2. Experiments were performed using cells up to the third passage.

Human pulmonary artery endothelial cells (PAEC) were isolated from surgical fragments. Segments of human arterial pulmonary endothelial cells (PAEC) were rinsed three times with a solution made of 3.9% saline containing 1% penicillin/streptomycin and fungizone (0.25 mg/mL) in order to remove blood cells and other contaminants. Specimens were then washed three times with 3.9% saline containing 250 μg/mL linezolid, 50 U/mL colistin, 25 μg/mL co-trimoxazole and 25 μg/mL amphotericin B and thereafter placed in 50 mL tubes containing DMEM/M199 (50%/50%), 10% FBS, 1% L-Glutamine (200 mmol/L), 1% Penicillin/Streptomicin (100 ×), 1% Fungizone (0.25 mg/mL), 1% ECGF (100 ×), 1% heparin (100 ×) plus 250 μg/mL linezolid, 50 U/mL colistin, 25 μg/mL co-trimoxazole and 25 μg/mL amphotericin B. Samples were maintained at 4 °C until exposed (usually

within 6–12 h from surgical excision) for 20 min at 37 °C, 5% CO_2, 90% humidity to phosphate-buffered saline (PBS) without calcium and magnesium containing 2 mg/mL type II collagenase (Worthington Biochem, Lakewood, NJ). Immediately after the incubation, samples were moved into a Petri dish (100 mm) containing culture medium (DMEM-M199, 50% vol/vol), supplemented with 10% FBS, 1% L-Glutamine, 1% Penicillin/Streptomicin, 1% Fungizone, 1% ECGF, 1% heparin (EC medium), together with 250 μg/mL linezolid, 50 U/mL colistin, 25 μg/mL co-trimoxazole and 25 μg/mL amphotericin B, which were progressively reduced and removed after a week from the explant. The artery fragments were massaged with a spatula followed by gentle shacking to detach the endothelial cells, which were collected by centrifugation at 330 x g for 7 min at room temperature. The cell pellet was suspended with EC medium and seeded on fibronectin (1 mg/cm²) (Sigma-Aldrich, Saint Louis, MO, USA)-coated cell culture dishes. Cells were maintained at 37 °C, 5% CO_2, 90% until confluent. With this method, the percentage of cells expressing the endothelial phenotype was variable from 10 to 50%.

To obtain a virtually pure endothelial population, we enriched EC using a method developed in our laboratory, based on early adhesion of EC compared to contaminant cells [17], which gave 95–98% endothelial cells after 3–4 passages. The endothelial phenotype was assessed by immunofluorescence (Suppl. Fig. 1). To this end, 2×10^4 cells were seeded on glass coverslips pre-coated with 1.5% gelatin. The next day cells were washed with PBS, fixed with 4% paraformaldehyde, permeabilized with 0.5% saponin and stained overnight at 4 °C with anti VWF (MA5-14029 Pierce) and CD31 (M0823 Dako) antibodies. Cells were subsequently exposed to Alexa Fluor® 488-labeled goat anti-Mouse IgG for 1 h at 4 °C. Draq-5 was used for nuclei staining. High definition images were acquired using a Zeiss LSM-510 META system (Carl Zeiss, Jena, Germany), equipped with a Zeiss Axiovert 200 inverted microscope.

2.2. CFTR expression

2.2.1. Western blotting

Cells were harvested and scraped into lysis buffer (50 mmol/L Tris, pH 7.4, 150 mmol/L NaCl, 1% Triton, 1% deoxycholate, 0.1% SDS) supplemented with protease inhibitors (Roche, Indianapolis, IN, USA). Lysates were incubated in a rocking platform for 30 min at 4 °C and then centrifuged at 13,000 rpm for 30 min at 4 °C to remove debris. Proteins were quantitated with a BCA protein assay kit (Thermo Scientific, Rockford, IL, USA), separated by SDS-PAGE and transferred on nitrocellulose membrane. After exposure to 5% nonfat milk in PBS for 1 h, membranes were probed with a specific primary antibody: anti-CFTR mAb clones L12B4 and M3A7 (1:100 each; Merck Millipore, Darmstadt, Germany). Anti-α-tubulin mAb (1:4000; Sigma-Aldrich, St. Louis, MO, USA) was used as loading control. The binding of primary antibodies was detected with anti-mouse secondary peroxidase-conjugated antibody (1:1000 to detect CFTR, 1:7500 for α-tubulin; Merck Millipore), and visualized with the clarity western ECL substrate (Bio-Rad, Hercules, CA, USA). Immunoblot images were acquired with Alliance 4.7 (UVITEC, Cambridge, UK). The intensity of the relevant bands was evaluated using the UVI band software package or with the ImageJ NIH Image Analysis Program.

2.2.2. Flow cytometry

CFTR expression in non-CF and CF-PAEC was also evaluated by flow cytometry. For surface localization, cells were detached with EDTA and collected by centrifugation (300 × g for 10 min). Pellets were suspended with PBS and incubated (1 h at 4 °C) with a mouse monoclonal anti-human CFTR antibody (CF3) (ThermoFisher) directed against the amino acid residues 103–107 located within the first extracellular loop. After removing the excess of primary antibody by centrifugation wash, cells were incubated with PerCP/Cy5.5-conjugated anti-mouse IgM (BioLegend, San Diego, CA, USA) for 1 h at 4 °C. For evaluation of

intracellular CFTR, cells were harvested, fixed with 3% formalin and permeabilized with FACS lysing and Perm2 solutions (BD) before staining. Cells were incubated with PBS containing an appropriate amount of the CFTR antibody MAB25031 (R & D Systems, Minneapolis, USA), for 1 h at 4 °C. They were then stained with Alex-Fluor 647 anti-mouse IgG (Invitrogen), as secondary antibody. Secondary antibody-matched controls were used to assess unspecific fluorescence.

2.3. CFTR activity

2.3.1. Whole-cell patch-clamp recording

Experiments were performed using a Multiclamp 700B amplifier (Axon Instruments, Molecular Devices, Sunnyvale, CA, USA) and an upright BX51WI microscope (Olympus, Japan) equipped with Nomarski optics. Patch electrodes, fabricated from thick borosilicate glasses, were pulled to a final resistance of 4–6 MΩ. Recordings with leak current < 100 pA and series resistance > 20 MΩ were discarded. All recordings were acquired at 50 kHz. Cl$^-$ currents were elicited by stepping from a holding potential of − 110 mV to + 110 mV with 10 mV increments in voltage clamp configuration. PAEC and CF-PAEC seeded at 35.000 cells/35 mm petri dishes were bathed in a solution containing: 140 mmol/L N-methyl D-glucamine; 140 mmol/L HCl; 2 mmol/L CaCl$_2$; 1 mmol/L MgCl$_2$ and 10 mmol/L HEPES (pH 7.4). Pipettes were filled with a solution containing: 140 mmol/L N-methyl D-glucamine; 40 mmol/L HCl; 100 mmol/L L-glutamic acid; 0.2 mmol/L CaCl$_2$; 2 mmol/L MgCl$_2$; 1 mmol/L EGTA; 10 mmol/L HEPES; 2 mmol/L ATP-Mg (pH 7.2). To activate CFTR conductance, a cAMP-activating cocktail (400 mmol/L cAMP, 10 mmol/L forskolin, 1 mmol/L IBMX) was added to the pipette solution. Acquisition and data analyses were performed using the pCLAMP 10.0 and Clampfit 10.0 software, respectively (Axon Instruments). Statistical analyses were carried out using Prism 5.0 software (GraphPad Software, San Diego, CA, USA).

2.3.2. Yellow fluorescent protein (YFP)

HUVEC were transfected with the Cl$^-$-sensitive YFP-encoding vector and plated onto 35 mm fibronectin-coated glass slides. Forty eight hours post transfection, cells were incubated in a NaCl (137 mmol/L)-containing buffered solution with Forskolin (20 mmol/L) plus or minus CFTRinh-172 (10 µmol/L) for 20–30 min. At the indicated time points, NaCl buffer was replaced with a NaI (137 mmol/L)-containing medium plus or minus CFTRinh-172 (10 µmol/L). The signal decay caused by YFP quenching as the consequence of the Cl$^-$/I$^-$ exchange was monitored using an upright fluorescence microscope (Zeiss), equipped with a Xenon lamp-based Optoscan monochromator (Cairn), a 20 × W Plan-Apochromat (N.A.: 1.0; Zeiss) objective and a 16-bit Evolve 512 EMCCD camera (Photometrics). Image acquisition and storage for offline analysis were performed by using Metamorph 7.7 software (Molecular Devices).

2.4. Endothelial permeability

Permeability to FITC-dextran of EC monolayers was assessed as previously reported [18]. Briefly, EC were grown to confluency on gelatin-coated translucent PET membrane porous filters (3 µm pores) (BD Falcon) and exposed to CFTRinh-172 (10 µmol/L) or DMSO in medium containing 10% serum for 24 h. Where indicated, IL-1β (5 ng/mL) was added to cells, 4 h before FITC-dextran (0.5 mg/mL, final concentration). RNO (100 nmol/L), cilostamide (10 µmol/L) and formoterol (100 nmol/L) were added 30 min before CFTRinh-172. FD4 (0,5 mg/mL) was added to the upper compartment of the transwells. At the indicated times, aliquots of medium (25 µL/well) were collected from the lower chamber and the amount of FITC-dextran was evaluated with a fluorimeter plate reader (Pharos, BIO-RAD).

2.5. Transendothelial electric resistance (TEER)

Non-CF-PAEC, exposed or not to 10 µmol/L CFTRinh-172 for 4 h at 37 °C, as well as CF-PAEC were seeded in gelatin-coated 0.4 µm polyester membrane transwell inserts (Corning, Tewksbury MA, USA) at 0.4 × 10^5 cells/well density in complete medium. TEER measurements were carried out when cells reached confluence. In some experiments, cells were treated with CFTRinh-172 (10 µmol/L) (Calbiochem) for 30 min before addition of IL-1β (10 ng/mL) (Peprotech, Rocky Hill, NJ, USA) and a mixture of roflumilast N-oxide (RNO) (100 nmol/L) and formoterol (100 nmol/L). TEER was measured at the indicated time after treatment by placing the electrodes at the upper and lower chambers. TEER was recorded at three different points of the sample cup. Inserts containing medium alone and untreated cells were used as blank and baseline resistance, respectively. The TEER was calculated subtracting the blank resistance from the resistance recorded in the presence of the cells.

2.6. Shear stress

EC were subjected to a shear stress of 5 dyne/cm^2 for 30 min as previously reported [16]. Briefly, EC, grown to confluency on gelatin-coated glass slides, were placed in a flow chamber under a microscope within a thermoregulated plexiglass box maintained at 37 °C. Endothelial cells were perfused with Hepes-buffered DMEM at a shear stress of 5 dyne/cm^2 for 30 min using a syringe pump (Harvard pump) and observed by phase contrast microscopy at 20 × magnification. Images were continuously video-recorded (Pro-Series video camera, High Performance CCD camera, Media Cybernetics, Silver Spring, MD, USA) and analyzed off-line. The number of cells showing morphological alterations was evaluated at the end of perfusion. The perfusion medium was collected to enumerate EMV by flow cytometry. At the end of perfusion, EC were fixed with 4% paraformaldehyde for confocal microscopy analysis (see below).

2.7. Adherence junction analysis

The distribution of VE-cadherin, p120-catenin, paxillin and vinculin in EC was assessed by confocal microscopy. EC were fixed in 4% PFA for 15 min at 37 °C and permeabilized with 0,1% saponin in PBS. The distribution of VE-cadherin, p120-catenin, paxillin and vinculin was assessed using rabbit polyclonal or mouse monoclonal antibodies. Alexa488-conjugated anti-rabbit or anti-mouse Ig antibodies were used for immunodetection. F-actin was detected by staining with rodhamine-conjugated phalloidin diluted 1:50 in phosphate buffer. Images were acquired using an LSM 510 confocal microscopy (Zeiss), equipped with a × 63 oil immersion objective with appropriate filter sets.

2.8. EMV analysis and enumeration

EMV were identified and numerated by flow cytometry, using a reported method [19]. EMV scatter properties were confirmed by running Megamix Plus beads (Biocytex, Marseille, France) at the same photomultiplier (PMT) voltages used for MV detection. Data were analyzed using FACSDiva v 6.1.3 (BD), FACSuite v 1.0.5 (BD) and FlowJo v 8.8.6 (TreeStar, Ashland, OR, USA) software. EMV number was obtained by volumetric count.

2.9. IL-8 measurements

IL-8 was determined in cell supernatants using a commercially available ELISA kit (R & D Systems, Minneapolis, MN, USA). HUVEC were cultured in DMEM and M-199 (50:50) supplemented with fetal bovine serum (20% vol/vol), bovine brain extract endothelial cell growth factor (ECGF, 50 µg/mL), and heparin (18 I U/mL) (Eparina Vister, Marvecs Pharma, Milan, Italy). Cells (1 × 10^5/well) between
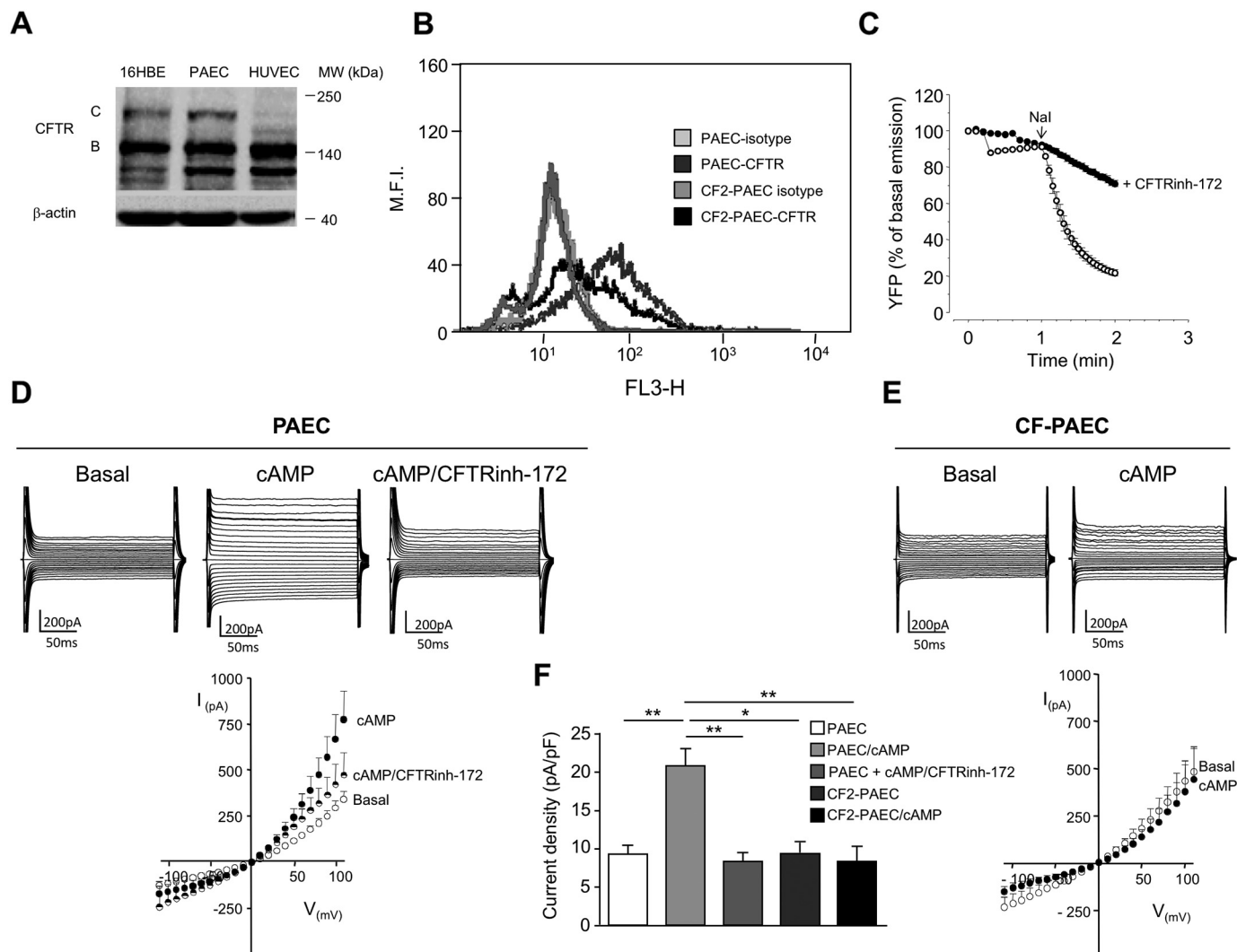
Fig. 1. CFTR expression and activity in endothelial cells.
(A) Western blotting. Thirty micrograms of total protein lysate from PAEC and 16HBE were blotted on nitrocellulose membrane. Immunodetection was performed with anti-human CFTR C-terminus antibody clone 24-1 (MAB25031, R & D systems) and anti-CFTR clone M3A7 (05-583, Upstate/Millipore). Each primary antibody was diluted at 1:500. Secondary Anti-Mouse Peroxidase conjugate antibody was used at 1:3000 dilution. (B) Flow cytometry. Membrane CFTR was determined in cells, stained with anti-CFTR Ab that recognizes amino acid residues 103-117 in the first extracellular loop of human and rabbit CFTR (MA1-935 IgM, Pierce, 1:100). Histograms depict isotype and anti-CFTR staining of PAEC and CF2-PAEC. (C) CFTR activity in HUVEC. HUVEC (0.5×10^6 cells) were transfected with the Cl^- sensitive YFP-encoding vector (1 μg) using the Amaxa Nucleofector kit (program U001). Forty eight hours post transfection, cells were incubated in a NaCl (137 mmol/L) buffered solution containing Forskolin (20 μmol/L) plus or minus CFTRinh-172 (10 μmol/L) for 20–30 min at 37 °C and YFP fluorescence intensity was measured for 1 min before replacement of NaCl with a NaI (137 mmol/L) buffer plus or minus CFTRinh-172 (10 μmol/L). The signal decay caused by YFP quenching due to the Cl^-/I^- exchange was monitored for 1 min.

passage 3 and 5 were seeded in 6-well plates and treated 24 h after reaching 90% confluence. Confluent cell monolayers were washed twice with DPBS, fresh medium consisting of DMEM:M-199 (50:50) plus 0.5% endotoxin free bovine serum albumin (BSA) was added, and cells recovered at 37 °C for 30 min. HUVEC were treated with CFTR-172 (10 μmol/L) (10 min) followed by TNF-α (0.5 μg/mL, Peprotech, London, UK). After 4 h, the supernatants were collected, centrifuged ad used for ELISA measurements.

2.10. Nitric oxide determination

Nitric oxide (NO) production by HUVEC was determined as previously reported [20]. Briefly, HUVEC, between the third and fifth passage, were grown to confluence at 1.5×10^4 in 6 multi-well plates using a medium enriched with 20% FCS, 10 μg/mL heparin and 50 μg/mL ECGF. Cells were made quiescent with 0.5% FBS for 2 h and then stimulated with 100 nmol/L insulin or 2 μmol/L ionomycin for 15 min at 37 °C. When present L-Name was added 40 min before the stimulus,

whereas CFTRinh-172 (10 μmol/L) was added to cells 10 min before the stimulus. At the end of the incubation, HUVEC were collected with a Hepes-Na + buffer containing $CaCl_2$. NO production was evaluated by conversion of L-(^{3}H)-arginine into L(^{3}H)-citrulline.

2.11. eNOS and AKT phosphorylation

eNOS phosphorylation was evaluated by flow cytometry. To this end, 1×10^6 cells/sample were washed and fixed with 1 mL FACS Lysing solution (BD Biosciences). Cells were permeabilized and incubated for 30 min at 4 °C in the dark with the primary antibody mix containing PBS 1X + total eNOS (1:500) and phospho eNOS (Ser1177, 1:500). After incubation with the secondary antibody mix (PBS 1X + Alexa 488 anti-mouse 1:1500, Alexa 488 anti-rabbit 1:1500) for 30 min at 4 °C in the dark, cells were washed and suspended with 500 μL PBS 1X. Cells were analyzed with a FACSCanto II flow cytometer (three lasers, eight-color configuration), equipped with the FACSDiva software v.6.1.3 (BD Biosciences).

For AKT phosphorylation, cell lysates (30 μg) were immunoblotted with anti-AKT (Cell Signaling Technology Inc.), anti-Ser473-Akt (Cell Signaling Technology, Inc.) and β-actin (Sigma-Aldrich) primary antibodies, followed by peroxidase-conjugated secondary antibodies. Proteins were detected using enhanced chemiluminescence and quantified with a computerized densitometric system. Data of AKT phosphorylation were normalized against total AKT content. Autoradiographs were quantified using the Molecular Analyst software (Bio-Rad Laboratories).

2.12. Statistical analysis

Only 2-tailed probabilities were used for testing statistical significance, and p < 0.05 was considered statistically significant.

3. Results

3.1. CFTR expression and activity in EC

CFTR expression was evaluated by western blotting and flow cytometry. Both HUVEC and PAEC express the mature form of CFTR (band C), which was more evident in PAEC (Fig. 1A). Membrane CFTR was assessed by flow cytometry (Fig. 1B). CFTR activity was evaluated by YFP fluorescence quenching in HUVEC (Fig. 1C) and patch clamping in PAEC (Fig. 1D). Electrophysiological recordings in whole cell configuration showed the induction of chloride currents by a cAMP-increasing cocktail (cAMP). This effect was blocked by CFTRinh-172, a selective CFTR inhibitor [21] (Fig. 1D). CFTR expression and activity was also determined in PAEC isolated from the explanted lungs of two CF patients with the following genotypes: G542X/1717-1G- > A (CF1) and F508del/F508del (CF2) (Suppl. Fig. 1). As expected, these cells had reduced membrane CFTR (Fig. 1B). Consistent with this, CF2-PAEC did not respond to cAMP (Fig. 1E), which instead enhanced PAEC current density (pA/pF) (Fig. 1F).

(D-F) Whole-cell patch clamping. Representative chloride currents in PAEC (D), either left untreated (Basal), or exposed to cAMP-increasing agents (cAMP) alone or in combination with CFTRinh-172 (10 μmol/L) or in CF-PAEC (E) exposed or not to cAMP. Currents were recorded in 200 ms voltage steps from −110 to +110 mV with 10 mV increments from a holding potential of −40 mV. Averaged current/voltage relationship in PAEC (n = 16); PAEC + cAMP (n = 15); PAEC + cAMP/CFTRinh-172 (n = 14); CF-PAEC (n = 10); CF-PAEC + cAMP (n = 10) are shown in the lower panels of (D) and (E), respectively. (F) Bars show chloride current density (pA/pF) recorded at +110 mV in the same samples of panel (D) and (E). Data are mean ± SEM. *p < 0.05; **p < 0.01, One Way Anova (Kruskal-Wallis test).

3.2. CFTR regulates endothelial barrier function

Since CFTR controls epithelial monolayer integrity [22], we investigated CFTR impact on EC permeability to macromolecules and transendothelial electrical resistance (TEER). CFTRinh-172 significantly increased cell permeability to dextran and reduced TEER (Fig. 2A and B). Remarkably, CF2-PAEC displayed lower basal TEER compared to normal PAEC, in a similar range as PAEC exposed to CFTRinh-172 (Fig. 2B).

Changes in endothelial permeability mainly result from alterations of intercellular junctions. Using confocal microscopy, we analyzed the impact of CFTR blockade on expression and distribution of VE-cadherin and p120 catenin, main components of AJ in HUVEC. As expected, in untreated HUVEC, VE-cadherin formed a continuous ribbon at the cell periphery and wide reticular structures, likely corresponding to regions of intercellular membrane overlaps (Fig. 2C). We observed a similar pattern for p120 catenin (Fig. 2C). CFTR blockade altered the junctional structures, determining the appearance of numerous gaps between

adjacent cells, in which VE-cadherin and p120 catenin disappeared from the membrane. Consistent with this, areas of intercellular contact exhibited reduced VE-cadherin and p120 catenin accumulation as well as reduced extension of reticular structures, being these effects more pronounced in IL-1β-treated HUVEC (Fig. 2C).

3.3. CFTR blockade alters endothelial stability under shear stress

To assess the impact of CFTR dysfunction in a more physiological setting, we subjected HUVEC and PAEC to shear forces (5 dyne/cm^2, 30 min). Untreated HUVEC retained their cobblestone-like appearance and tight intercellular membrane apposition (Video 1).

In contrast, CFTRinh-172-treated cells showed significant alterations of cell morphology and intercellular junctions. A significant number of EC displayed membrane blebs at the apical surface and cellular edges. Blebbing evolved into shrinking of the cell body, disruption of cell-cell contacts and opening of intercellular gaps (Video 2).

These events were more pronounced in IL-1β-treated HUVEC (Videos 3 and 4).

PAEC subjected to shear showed a similar behavior (Videos 5 and 6).

CFTRinh-172 increased the number of EC undergoing morphological alterations after 30 min perfusion in unstimulated (3.6 ± 0.8 vs 17.3 ± 2.0/cells per field; p < 0.05) and IL-1β-treated EC (7.2 ± 0.8 vs 35.4 ± 1.9/cells per field; p < 0.05) (Fig. 3A). Such changes were not appreciated in the absence of shear (results not shown).

We also analyzed the organization of the endothelial junctions under shear. HUVEC subjected to shear exhibited VE-cadherin distribution at the cell periphery, organized in reticular structures at intercellular membrane overlaps (Fig. 3B). CFTRinh-172 induced the formation of gaps between adjacent cells, in which the accumulation of VE-cadherin was reduced (Fig. 3B). These effects were more pronounced in the presence of IL-1β (Fig. 3B). Notably, paxillin and vinculin, two focal adhesion (FA)-associated proteins, accumulated inside the blebs (Fig. 3C). This is consistent with the hypothesis that CFTR dysfunction can affect the functional integrity of FA in EC.

3.4. CFTR loss-of-function alters EMV release and activity

Membrane blebs are usually associated with the formation of MV. EMV are released during inflammation or apoptosis and regarded as biological indices of endothelial dysfunction [23]. We, therefore, collected and enumerated EMV in media from HUVEC or PAEC exposed or not to CFTRinh-172. CFTR blockade clearly stimulated EMV generation both by resting and IL-1β-treated cells (Fig. 4A). Consistent with this, CF2-PAEC released a higher number of EMV (CF-EMV), compared to non-CF PAEC (Fig. 4B). In contrast to EMV from non-CF PAEC, CF-EMV were unable to stimulate proliferation of recipient PAEC or CF2-PAEC (Fig. 4C). This effect was not related to differences in EMV uptake by recipient cells (results not shown).

3.5. cAMP-increasing agents correct the loss of EC barrier function triggered by CFTR blockade

The cAMP/PKA signaling is key for the maintenance of the endothelial barrier function [24]. The cAMP pool is physiologically controlled by the combined action of type 3 and 4 phosphodiesterases (PDE) and adenylyl cyclase. Also, the activation of β-adrenergic receptors stimulates adenylyl cyclase and improves endothelial barrier function in vitro and in vivo [25]. On the other hand, PDE inhibitors and β-adrenergic agonists have been reported to improve CFTR activity in epithelial cells as well as in murine hematopoietic stem/progenitor cells [26,27]. Based on this evidence, we evaluated the efficacy of selective PDE3 and PDE4 inhibitors in combination with a β$_2$-adrenergic agonist to counteract CFTR blockade-induced endothelial dysfunction.
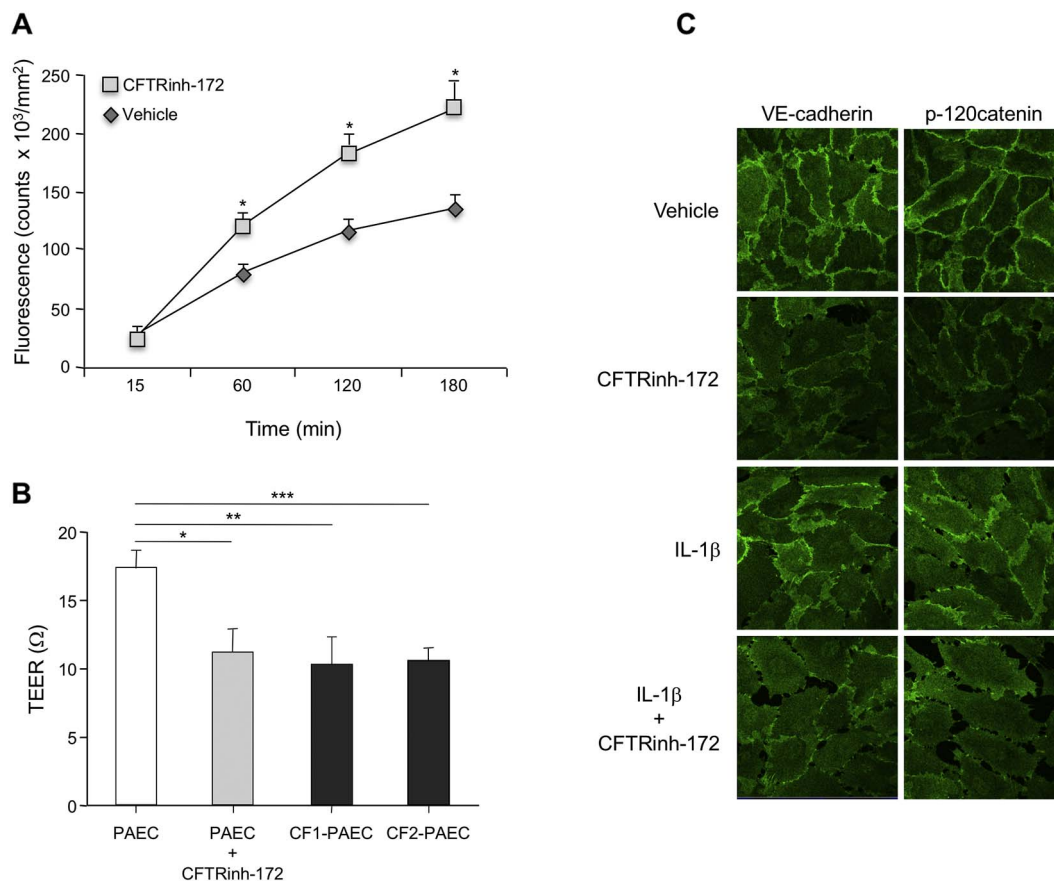
Fig. 2. CFTR loss-of-function increases EC permeability, while reducing TEER and VE-cadherin and p120-catenin membrane expression.
(A) Confluent HUVEC, grown on culture inserts (3 μm pore size) set into 12 well plates, were incubated in the presence of CFTRinh-172 (10 μmol/L) or DMSO vehicle. After 24 h, FITC-dextran (0.5 mol/L) was added to the upper compartment. At the indicated times, aliquots (25 μL) of medium were collected from the lower compartment and their fluorescence monitored with the Pharos Fx, Molecular Imager. Results are expressed as Arbitrary Fluorescence Units (counts $\times 10^3/mm^2$). The graph shows mean $\pm$ SEM; n = 5; *p < 0.05 (Student *t*-test vs DMSO). (B) Confluent PAEC were exposed to DMSO or CFTRinh-172 (10 μmol/L) for 4 h. CF1-PAEC (G542X/1717-1G- > A) and CF2-PAEC (F508del/F508del) were examined in parallel. TEER was measured using an EVOM analyzer as reported in methods. Resistance was expressed in Ohm (Ω) subtracting blank values. Results are mean $\pm$ SEM from 3 measurements at different passage with duplicates; *p = 0.0088; **p = 0.0063; ***p = 0.0028. (C) Confluent HUVEC, grown on culture slides, were exposed to CFTRinh-172 (10 μmol/L) or DMSO for 24 h. IL-1β (5 ng/mL) was added to cells 4 h before fixation with 4% paraformaldheyde. HUVEC were permeabilized and stained for VE-cadherin or p120-catenin, using specific polyclonal antibodies. Confocal microscopy images were acquired at × 630 magnification. Images are representative of n = 3 experiments.

Treatment with a combination of cilostamide (PDE3 inhibitor), roflumilast N-oxide (RNO) (PDE4 inhibitor) and formoterol, a long acting β2-adrenergic agonist, corrected permeability and TEER, both in PAEC exposed to CFTRinh-172 and CF1-PAEC (Fig. 5A–C), and reduced VE-cadherin and p120 catenin alterations at the intercellular junctions in CFTRinh-172-treated EC, both, under basal or inflammatory conditions (Fig. 5D). Remarkably, under shear these agents abrogated alterations in cell morphology and monolayer integrity, triggered by CFTR blockade in HUVEC (Fig. 5D,E and Videos 7,8) as well as in PAEC (Videos 9,10).

3.6. CFTR controls key endothelial-dependent regulatory mechanisms of vascular tone and leukocyte recruitment

To obtain further evidence of CFTR signaling in endothelial cells, we evaluated the impact of CFTR blockade on two main endothelial-derived modulators of the vascular tone and inflammation, namely NO and IL-8. CFTR blockade suppressed insulin-induced NO generation by HUVEC (Fig. 6A). This was related to the inhibition of eNOS and AKT phosphorylation (Fig. 6B and C). On the other hand, CFTR blockade significantly enhanced IL-8 release by EC (Fig. 6D). These results indicate that endothelial cells expressing a dysfunctional CFTR, acquire a phenotype compatible with increased vascular tone and excessive PMN recruitment, thus contributing to sustain inflammation.

4. Discussion

The concept of CF as a systemic disorder affecting different cells, tissues and functions has been recently reinforced by the evidence of CFTR expression and activity in a variety of cells. We uncovered CFTR in platelets [5], whereas CFTR expression and activity has been observed in leukocytes [6,7], smooth muscle cells [28] and stem cells [29]. Moreover, conditional knockouts have provided valuable information on CFTR bioactions and signaling in non-respiratory cells [30,31].

Here, we examined CFTR expression and function in EC. Since little was known regarding endothelial functions controlled by CFTR in EC, we undertook a horizontal approach by exploring the consequences of CFTR loss-of-function on a variety of EC key regulatory activities of vascular homeostasis and inflammation. For this scope, we employed EC isolated for the first time from fragments of the pulmonary artery from explanted CF lungs [17] and compared data with normal EC cells exposed to CFTRinh-172 as an in vitro pharmacological model of CF. CFTR activity in these cells was carefully evaluated (Fig. 1D–F) and the two models were always consistent.

Based on CFTR signaling in epithelial cells and histological analyses of CFTR lungs [22,32], we initially evaluated CFTR involvement in the regulation of endothelial barrier function. Data with HUVEC, PAEC and CF-PAEC were consistent to show that CFTR loss-of-function impaired the EC barrier function (Fig. 2A and B). This observation is in line with
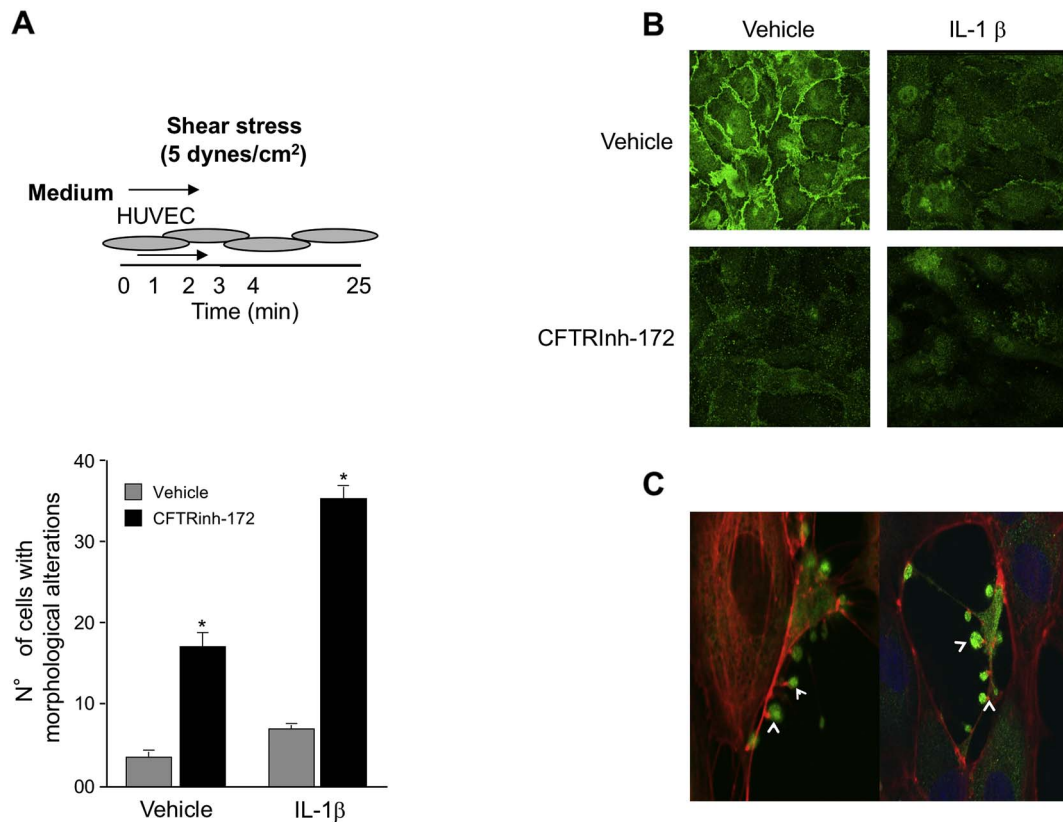
Fig. 3. Impact of CFTR blockade on EC under shear stress.
(A) Confluent, resting or IL-1β-treated (5 ng/mL, 4 h) HUVEC perfused (30 min) with DMEM containing CFTRinh-172 (10 μmol/L) or DMSO, at 5 dynes/cm² (upper panel). EC morphology was monitored during perfusion and video recorded. Cells that underwent morphologic alterations under shear were enumerated at the end of perfusion. Bars (lower panel) report the number of cells showing blebs, shrinking and retraction per optical field (0.7 mm²). Values are mean ± SEM; (n = 11 for resting and n = 53 for IL-1β-treated HUVEC); *p < 0.05 vs vehicle (ANOVA for repeated measurements, Tukey test). (B) VE-cadherin membrane expression. HUVEC were treated as in A, fixed with 4% paraformaldhehyde and permeabilized. VE-cadherin was visualized using a specific polyclonal antibody. Confocal microscopy images were acquired at ×630 magnification. The image is representative of n = 3. (C) Accumulation of paxillin (left) and vinculin (right) in CFTRinh-172-induced blebs. HUVEC were subjected to shear forces ad fixed as above. Paxillin and vinculin (green) were visualized using specific polyclonal antibodies and F-actin (red), by rhodamine-conjugated phalloidin. Images were acquired at ×630 magnification (CROP × 3). The image is representative of n = 3, with cells from umbilical cords from different donors.
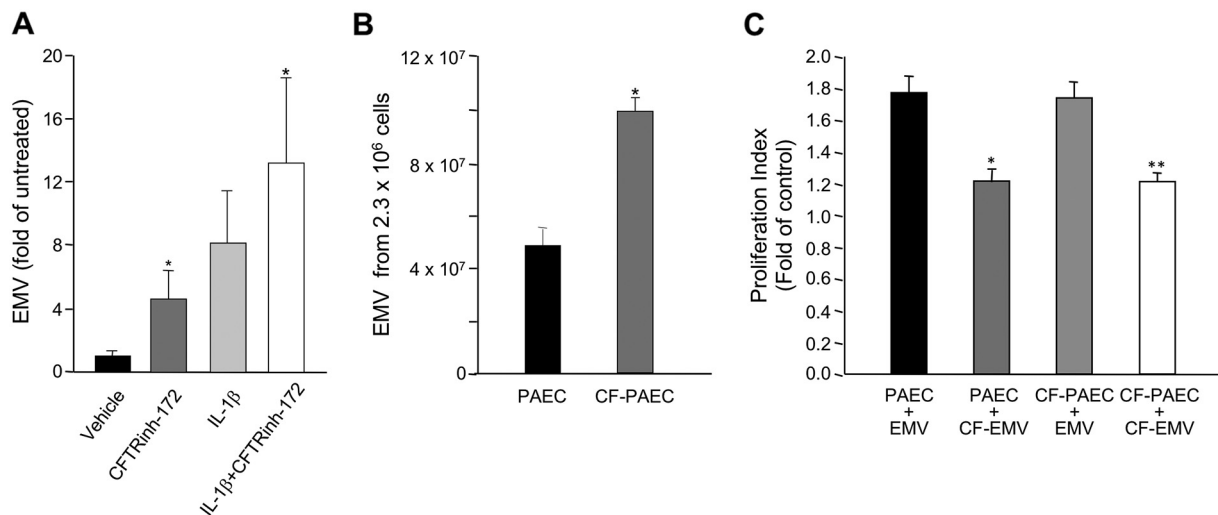
Fig. 4. EMV in CF. (A) HUVEC were exposed or not to IL-1β (5 ng/mL, 4 h), CFTRinh-172 (10 μmol/L) or the combination of the two. Cells were subjected to 20 dynes/cm² shear for 40 min. Flow fluid (~50 mL) was collected and EMV were enumerated by flow-cytometry. Bars represent mean ± SD from n = 3. *p < 0.01. (B) Cells were grown for 48 h in 100 mm Petri dishes. The supernatant (~10 mL) was collected and EMV were counted by flow cytometry. Counts normalized for cell number. Bars represent mean ± SEM of 3 enumerations. *p = 0.004. (C) PAEC or CF-PAEC (2.4 × 10⁴) were incubated with EMV or CF-EMV (1:10) for 24 h in the presence of 2% FBS. Cells were counted and their viability was assessed by trypan blue staining. Results are mean ± SEM from n = 2 with duplicates. *p = 0.005 vs PAEC incubated with EMV; **p = 0.002 vs CF-PAEC incubated with EMV.
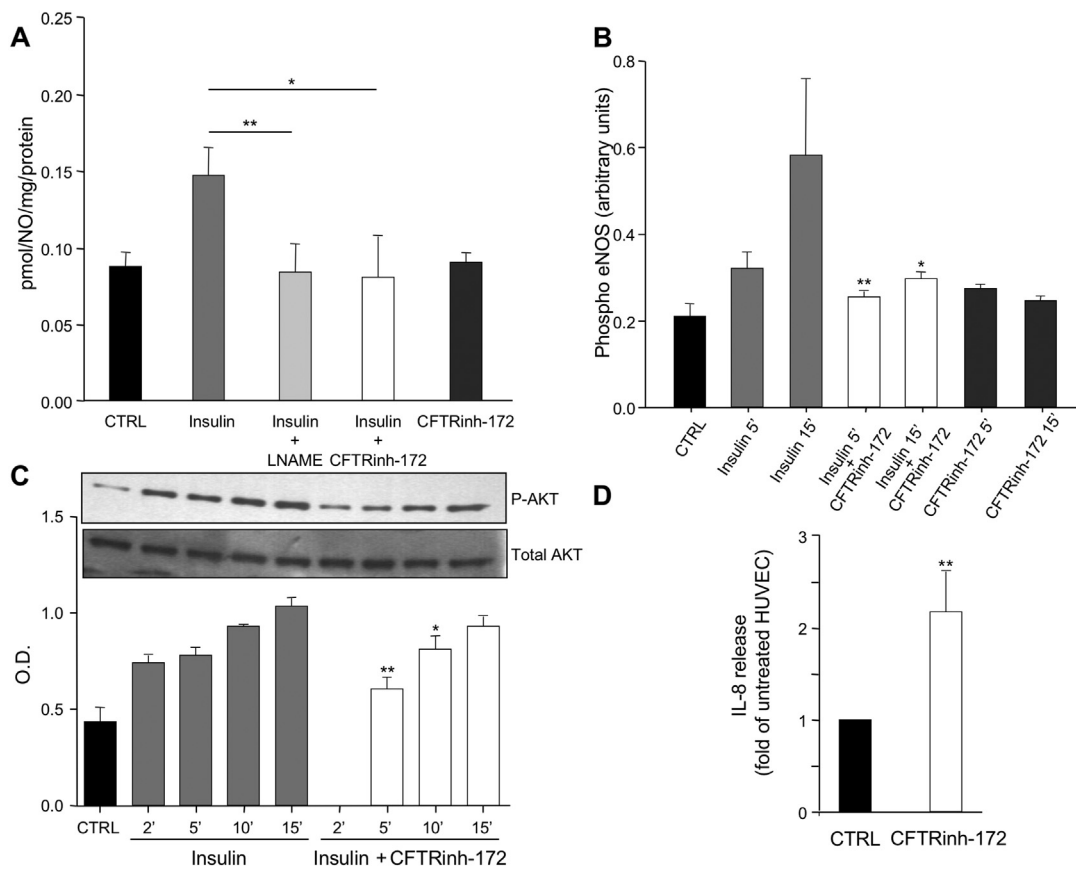
Fig. 6. CFTR inhibition blocks NO generation, eNOS and AKT phosphorylation, and stimulates IL-8 release.

(A) HUVEC (1.5×10^4) between the third and fifth passage, were grown in a medium containing 20% FCS, 10 μg/mL heparin and 50 μg/mL ECGF. Cells were made quiescent with 0.5% FBS for 2 h and then stimulated with 100 nmol/L insulin for 15 min at 37 °C. When present L-NAME was added 40 min before the stimulus, whereas CFTRinh-172 (10 μmol/L) was added to cells 10 min before the stimulus. At the end of the incubation, HUVEC were collected with a Hepes-Na + buffer containing $CaCl_2$. NO production was evaluated by conversion of L-(^{3}H)-arginine into L-(^{3}H)-citrulline. Bars represent mean ± SD from n = 3 (*p = 0.017; **p = 0.0027). (B) HUVEC were exposed to insulin (100 nmol/L), in the presence or not of CFTRinh-172 (10 μmol/L) for the indicated time, and eNOS phosphorylation was evaluated by flow cytometry. To this end, 1×10^6 cells/sample was fixed with 1 mL FACS Lysing solution (BD Biosciences). Cells were permeabilized and incubated for 30 min at 4 °C in the dark with the primary antibody mix containing PBS 1X + total eNOS (1:500) and phospho eNOS (Ser1177, 1:500), followed by the secondary antibody mix (PBS 1X + Alexa 488 anti-mouse 1:1500, Alexa 488 anti-rabbit 1:1500). Cells were washed and analyzed with a FACSCanto II flow cytometer. Results are mean ± SD from n = 3 (*p = 0.048 vs Insulin 15′; **p = 0.046 vs Insulin 5′). (C) Cell lysates (30 μg) were immunoblotted with anti-Akt, anti-Ser473-Akt and β-actin primary antibodies, followed by peroxidase-conjugated secondary antibodies. Data of Akt phosphorylation were normalized for total Akt. Autoradiographs were quantitated using the Molecular Analyst software. Images from a representative experiment are reported in the upper panel. Bars represent mean ± SD from n = 3. ***p = 0.002 vs Insulin 2′; **p = 0.01 vs Insulin 5′; *p = 0.04 vs Insulin 10′; *p = 0.04 vs Insulin 15′. (D) HUVEC monolayers were exposed to CFTRinh-172 for 4 h. Medium was collected as assayed for IL-8 by ELISA. Bars represent mean ± SD of n = 4 (*p = 0.002).

cell proliferation as efficiently as EMV from non-CF cells. This is likely due to changes in content, since no changes in EMV uptake was detected (results not shown).

Altogether, our shear stress data support the view of CFTR being a sensor of cyclic strain that triggers integrated biochemical signaling aimed at coordinating physical cell adaptation and responses to mechanical stimuli, such as blood flow in the case of EC and respiratory cycles for epithelial cells. Indeed, airway epithelial cells respond to mechanical stress with the release of inflammatory mediators, such as oxygen radicals and cytokines, including IL-8, as well as with cytoskeleton re-organization [40].

Results from experiments with agents that increase cAMP may be helpful to define the signaling pathways underlying the CFTR-dependent control of EC barrier function. We consistently observed that the combination of PDE inhibitors and β-adrenergic agonists normalized EC integrity as well as VE-cadherin and p120 catenin distribution (Fig. 5 and Videos 8 and 10). These results may further support the use of these agents that can also directly stimulate CFTR activity [26,27], as a therapeutic option to normalize both epithelial and endothelial functions in CF patients. On the other hand, the present data suggest that at least some of the endothelial alterations consequent to CFTR-loss-of-function may be related to cAMP signaling. Indeed, that CFTR may act

as a multidirectional signal generator to many cellular pathways that involve cAMP is an emerging concept (reviewed by Kunzelmann & Mehta) [41]. Along these lines, CFTR regulation of PKA activation during sperm capacitation has been reported [42].

Having established that CFTR dysfunction profoundly affected EC dynamics, we next asked whether it could also modify functional indices, related to inflammation and vascular biology. We focused on NO, a main regulator of the vascular tone and inflammatory responses [43] observing that CFTR blockade suppressed insulin-induced NO generation by EC (Fig. 6). This is consistent with our early data with platelets [5] and with the observation of reduced nasal NO in CF patients [44]. Here, however, we provide a mechanistic background for the reduced NO production by CF patients, as we show that CFTR controls the phosphorylation and the activity of eNOS (Fig. 5), likely by acting on AKT phosphorylation (Fig. 5C). It has to be denoted that CFTRinh-172 did not alter calcium ionophore-induced NO release, suggesting that CFTR blockade may interfere with insulin signaling. This is consistent with recent data in CF airways [45]. Moreover, since CF patients often suffer from diabetes mellitus, mainly due to reduced CFTR-regulated insulin secretion [46], it is likely that CFTR-dependent changes in insulin sensitivity may play a role in this setting.

Together with data showing that CFTR expressed by vascular

smooth muscle cells is involved in the regulation of hypoxic pulmonary vasoconstriction [12], these results suggest that CFTR dysfunction is associated with the impairment of key vasoregulatory mechanisms, which may have pathogenetic consequences. Indeed, recent studies have pointed out the risk of cardiovascular events in CF patients [47]. These risks may be now more appreciable, due to the extension of the lifespan of these patients.

Interestingly, CFTR blockade upregulated IL-8 generation by EC (Fig. 5D). This confirms the acquisition of an inflammatory-prone phenotype by EC with dysfunctional CFTR, since IL-8 is a main chemotactic agent for PMN. It also supports the similarity in responses between epithelial and endothelial cells [48] and suggests that EC can significantly contribute to the increase in circulating IL-8 in CF patients [49].

In conclusion, we report that CFTR controls homeostatic functions of EC, providing insights into CFTR pathophysiology in the vascular endothelium. Although, we did not explore in detail the mechanisms involved in these, previously unappreciated, CFTR functions, the evidence that drugs that modulate cAMP signaling can protect EC from alterations triggered by CFTR dysfunction, while opening avenues for innovative pharmacological approaches to CF, suggests that at least some of the endothelial alterations triggered by CFTR-loss-of-function may be related to cAMP signaling.

Supplementary data to this article can be found online at http://dx.doi.org/10.1016/j.bbadis.2017.08.011.

Transparency document

The http://dx.doi.org/10.1016/j.bbadis.2017.08.011 associated with this article can be found, in the online version.

Acknowledgements

References

[1] J.R. Riordan, J.M. Rommens, B. Kerem, N. Alon, R. Rozmahel, Z. Grzelczak, J. Zielenski, S. Lok, N. Plavsic, J.L. Chou, M.L. Drumm, M.C. Iannuzzi, F.S. Collins, L.-C. Tsui, Identification of the cystic fibrosis gene: cloning and characterization of complementary DNA, Science 245 (1989) 1066–1073.

[2] M.P. Anderson, R.J. Gregory, S. Thompson, D.W. Souza, S. Paul, R.C. Mulligan, A.E. Smith, M.J. Welsh, Demonstration that CFTR is a chloride channel by alteration of its anion selectivity, Science 253 (1991) 202–205.

[3] J.H. Poulsen, H. Fischer, B. Illek, T.E. Machen, Bicarbonate conductance and pH regulatory capability of cystic fibrosis transmembrane conductance regulator, Proc. Natl. Acad. Sci. U. S. A. 91 (1994) 5340–5344.

[4] D.A. Stoltz, D.K. Meyerholz, M.J. Welsh, Origins of cystic fibrosis lung disease, N. Engl. J. Med. 372 (2015) 1574–1575.

[5] D. Mattoscio, V. Evangelista, R. De Cristofaro, A. Recchiuti, A. Pandolfi, S. Di Silvestre, S. Manarini, N. Martelli, B. Rocca, G. Petrucci, D.F. Angelini, L. Battistini, I. Robuffo, T. Pensabene, L. Pieroni, M.L. Furnari, F. Pardo, S. Quattrucci, S. Lancellotti, G. Davì, M. Romano, Cystic fibrosis transmembrane conductance regulator (CFTR) expression in human platelets: impact on mediators and mechanisms of the inflammatory response, FASEB J. 24 (2010) 3970–3980.

[6] P. Del Porto, N. Cifani, S. Guarnieri, E.G. Di Domenico, M.A. Mariggiò, F. Spadaro, S. Guglietta, M. Anile, F. Venuta, S. Quattrucci, F. Ascenzioni, Dysfunctional CFTR alters the bactericidal activity of human macrophages against *Pseudomonas aeruginosa*, PLoS One 6 (2011) e19970.

[7] R.G. Painter, V.G. Valentine, N.A. Lanson Jr., K. Leidal, Q. Zhang, G. Lombard, C. Thompson, A. Viswanathan, W.M. Nauseef, G. Wang, G. Wang, CFTR expression in human neutrophils and the phagolysosomal chlorination defect in cystic fibrosis, Biochemistry 45 (2006) 10260–10269.

[8] E. Dejana, M. Corada, M.G. Lampugnani, Endothelial cell-to-cell junctions, FASEB J. 9 (1995) 910–918.

[9] Xiao K1, Garner J, Buckley KM, Vincent PA, Chiasson CM, Dejana E, Faundez V, Kowalczyk AP., p120-Catenin regulates clathrin-dependent endocytosis of VE-cadherin, Mol. Biol. Cell 16 (2005) 5141–5151.

[10] S. Yamamoto, E. Azuma, M. Muramatsu, T. Hamashima, Y. Ishii, M. Sasahara, Significance of extracellular vesicles: pathobiological roles in disease, Cell Struct. Funct. 41 (2016) 137–143.

[11] A. Tousson, B.A. Van Tine, A.P. Naren, G.M. Shaw, L.M. Schwiebert, Characterization of CFTR expression and chloride channel activity in human endothelia, Am. J. Phys. 275 (6 Pt 1) (1998) C1555–564.

[12] C. Tabeling, H. Yu, L. Wang, H. Ranke, N.M. Goldenberg, D. Zabini, E. Noe, A. Krauszman, B. Gutbier, J. Yin, M. Schaefer, C. Arenz, A.C. Hocke, N. Suttorp, R.L. Proia, M. Witzenrath, W.M. Kuebler, CFTR and sphingolipids mediate hypoxic pulmonary vasoconstriction, Proc. Natl. Acad. Sci. U. S. A. 112 (2015) E1614–623.

[13] M. Romano, M. Collura, L. Lapichino, F. Pardo, A. Falco, P.L. Chiesa, G. Caimi, G. Davì, Endothelial perturbation in cystic fibrosis, Thromb. Haemost. 86 (2001) 1363–1367.

[14] S. Poore, B. Berry, D. Eidson, K.T. McKie, R.A. Harris, Evidence of vascular endothelial dysfunction in young patients with cystic fibrosis, Chest 143 (2013) 939–945.

[15] P. Rodriguez-Miguelez, J. Thomas, N. Seigler, R. Crandall, K.T. McKie, C. Forseen, R.A. Harris, Evidence of microvascular dysfunction in patients with cystic fibrosis, Am. J. Physiol. Heart Circ. Physiol. 310 (2016) H1479–1485.

[16] L. Di Francesco, L. Totani, M. Dovizio, A. Piccoli, A. Di Francesco, T. Salvatore, A. Pandolfi, V. Evangelista, R.A. Dercho, F. Seta, P. Patrignani, Induction of prostacyclin by steady laminar shear stress suppresses tumor necrosis factor-alpha biosynthesis via heme oxygenase-1 in human endothelial cells, Circ. Res. 104 (2009) 506–513.

[17] R. Plebani, R. Tripaldi, P. Lanuti, A. Recchiuti, S. Patruno, S. Di Silvestre, P. Simeone, M. Anile, F. Venuta, M. Prioletta, F. Mucilli, P. Del Porto, M. Marchisio, A. Pandolfi, M. Mario Romano, Establishment and long-term culture of human cystic fibrosis endothelial cells, Lab. Invest. (2017), http://dx.doi.org/10.1038/labinvest.2017.74 (Epub ahead of print).

[18] G.P1. van Nieuw Amerongen, R. Draijer, M.A. Vermeer, V.W. van Hinsbergh, Activation of RhoA by thrombin in endothelial hyperpermeability: role of Rho kinase and protein tyrosine kinases, Circ. Res. 87 (2000) 335–340.

[19] P. Lanuti, F. Santilli, M. Marchisio, L. Pierdomenico, E. Vitacolonna, E. Santavenere, A. Iacone, G. Davì, M. Romano, S. Miscia, A novel flow cytometric approach to distinguish circulating endothelial cells from endothelial microparticles: relevance for the evaluation of endothelial dysfunction, J. Immunol. Methods 380 (2012) 16–22.

[20] A. Pandolfi, A. Grilli, C. Cilli, A. Patruno, A. Giaccari, S. Di Silvestre, M.A. De Lutiis, G. Pellegrini, F. Capani, A. Consoli, M. Felaco, Phenotype modulation in cultures of vascular smooth muscle cells from diabetic rats: association with increased nitric oxide synthase expression and superoxide anion generation, J. Cell. Physiol. 196 (2003) 378–385.

[21] T. Ma, J.R. Thiagarajah, H. Yang, N.D. Sonawane, C. Folli, L.J. Galietta, A.S. Verkman, Thiazolidinone CFTR inhibitor identified by high-throughput screening blocks cholera toxin-induced intestinal fluid secretion, J. Clin. Invest. 110 (2002) 1651–1658.

[22] P. LeSimple, J. Liao, R. Robert, D.C. Gruenert, J.W. Hanrahan, Cystic fibrosis transmembrane conductance regulator trafficking modulates the barrier function of airway epithelial cell monolayers, J. Physiol. 588 (Pt 8) (2010) 1195–1209.

[23] A.S. Leroyer, F. Anfosso, R. Lacroix, F. Sabatier, S. Simoncini, S.M. Njock, N. Jourde, P. Brunet, L. Camoin-Jau, J. Sampol, F. Dignat-George, Endothelial-derived microparticles: biological conveyors at the crossroad of inflammation, thrombosis and angiogenesis, Thromb. Haemost. 104 (2010) 456–463.

[24] H1. Lum, H.A. Jaffe, I.T. Schulz, A. Masood, A. RayChaudhury, R.D. Green, Expression of PKA inhibitor (PKI) gene abolishes cAMP-mediated protection to endothelial barrier dysfunction, Am. J. Phys. 277 (3 Pt 1) (1999) C580–588.

[25] V. Spindler, J. Waschke, Beta-adrenergic stimulation contributes to maintenance of endothelial barrier functions under baseline conditions, Microcirculation 18 (2011) 118–127.

[26] S. Liu, A. Veilleux, L. Zhang, A. Young, E. Kwok, F. Laliberté, C. Chung, M.R. Tota, D. Dubé, R.W. Friesen, Z. Huang, Dynamic activation of cystic fibrosis transmembrane conductance regulator by type 3 and type 4D phosphodiesterase inhibitors, J. Pharmacol. Exp. Ther. 314 (2005) 846–854.

[27] T. Trotta, L. Guerra, D. Piro, M. d'Apolito, C. Piccoli, C. Porro, I. Giardino, S. Lepore, S. Castellani, A. Petrella, A.B. Maffione, V. Casavola, N. Capitanio, M. Conese, Stimulation of β2-adrenergic receptor increases CFTR function and decreases ATP levels in murine hematopoietic stem/progenitor cells, J. Cyst. Fibros. 14 (2015) 26–33.

[28] C.A. Hübner, B.C. Schroeder, H. Ehmke, Regulation of vascular tone and arterial blood pressure: role of chloride transport in vascular smooth muscle, Pflugers Arch. 467 (2015) 605–614.

[29] D. Piro, C. Piccoli, L. Guerra, F. Sassone, A. D'Aprile, M. Favia, S. Castellani, S. Di Gioia, S. Lepore, M.L. Garavaglia, T. Trotta, A.B. Maffione, V. Casavola, G. Meyer, N. Capitanio, M. Conese, Hematopoietic stem/progenitor cells express functional mitochondrial energy-dependent cystic fibrosis transmembrane conductance regulator, Stem Cells Dev. 21 (2012) 634–646.

[30] T.L. Bonfield, C.A. Hodges, C.U. Cotton, M.L. Drumm, Absence of the cystic fibrosis transmembrane regulator (Cftr) from myeloid-derived cells slows resolution of inflammation and infection, J. Leukoc. Biol. 92 (2012) 1111–1122.

[31] C. Mueller, S.A. Braag, A. Keeler, C. Hodges, M. Drumm, T.R. Flotte, Lack of cystic fibrosis transmembrane conductance regulator in CD3 + lymphocytes leads to aberrant cytokine secretion and hyperinflammatory adaptive immune responses, Am. J. Respir. Cell Mol. Biol. 44 (2011) 922–929.

[32] J.F. Tomashefski Jr., C.R. Abramowsky, M. Chung-Park, J. Wisniewska, M.C. Bruce, Immunofluorescence studies of lung tissue in cystic fibrosis, Pediatr. Pathol. 112 (1992) 313–324.

[33] M.B. Brown, W.R. Hunt, J.E. Noe, N.I. Rush, K.S. Schweitzer, T.C. Leece, A. Moldobaeva, E.M. Wagner, S.M. Dudek, C. Poirier, R.G. Presson Jr., E. Gulbins, I. Petrache, Loss of cystic fibrosis transmembrane conductance regulator impairs lung endothelial cell barrier function and increases susceptibility to microvascular damage from cigarette smoke, Pulm. Circ. 4 (2014) 260–268.

[34] M. Trani, E. Dejana, New insights in the control of vascular permeability: vascular endothelial-cadherin and other players, Curr. Opin. Hematol. 22 (2015) 267–272.

[35] E. Dejana, F. Orsenigo, M.G. Lampugnani, The role of adherens junctions and VE-cadherin in the control of vascular permeability, J. Cell Sci. 121 (Pt 13) (2008) 2115–2122.

[36] H.E. de Vries, M.C. Blom-Roosemalen, M. van Oosten, A.G. de Boer, T.J. van Berkel, D.D. Breimer, J. Kuiper, The influence of cytokines on the integrity of the blood-brain barrier in vitro, J. Neuroimmunol. 64 (1996) 37–43.

[37] X. Zhong, J. Drgonova, C.Y. Li, G.R. Uhl, Human cell adhesion molecules: annotated functional subtypes and overrepresentation of addiction-associated genes, Ann. N. Y. Acad. Sci. 1349 (2015) 83–95.

[38] A.A. Birukova, I. Cokic, N. Moldobaeva, K.G. Birukov, Paxillin is involved in the differential regulation of endothelial barrier by HGF and VEGF, Am. J. Respir. Cell Mol. Biol. 40 (2009) 99–107.

[39] C. Porro, S. Lepore, T. Trotta, S. Castellani, L. Ratclif, A. Battaglino, S. Di Gioia, M.C. Martínez, M. Conese, A.B. Maffione, Isolation and characterization of micro-particles in sputum from cystic fibrosis patients, Respir. Res. 11 (2010) 94.

[40] C.M. Waters, E. Roan, D. Navajas, Mechanobiology in lung epithelial cells: measurements, perturbations, and responses, Compr. Physiol. 2 (2012) 1–29.

[41] K. Kunzelmann, A. Mehta, CFTR: a hub for kinases and crosstalk of cAMP and Ca2 +, FEBS J. 280 (2013) 4417–4429.

[42] L.C. Puga Molina, N.A. Pinto, P. Torres Rodríguez, A. Romarowski, A. Vicens Sanchez, P.E. Visconti, A. Darszon, C.L. Treviño, M.G. Buffone, Essential role of CFTR in PKA-dependent phosphorylation, alkalinization, and hyperpolarization during human sperm capacitation, J. Cell. Physiol. 232 (2016) 1404–1414.

[43] J.L. Wallace, A. Ianaro, K.L. Flannigan, G. Cirino, Gaseous mediators in resolution of inflammation, Semin. Immunol. 27 (2015) 227–233.

[44] R.K. Michl, J. Hentschel, C. Fischer, J.F. Beck, J.G. Mainz, Reduced nasal nitric oxide production in cystic fibrosis patients with elevated systemic inflammation markers, PLoS One 8 (2013) e79141.

[45] S.A. Molina, H.K. Moriarty, D.T. Infield, B.R. Imhoff, R.J. Vance, A.H. Kim, J.M. Hansen, W.R. Hunt, M. Koval, N.A. McCarty, Insulin signaling via the PI3-kinase/Akt pathway regulates airway glucose uptake and barrier function in a CFTR-dependent manner, Am. J. Phys. Lung Cell. Mol. Phys. 312 (2017) L688–L702.

[46] J.H. Guo, H. Chen, Y.C. Ruan, X.L. Zhang, X.H. Zhang, K.L. Fok, L.L. Tsang, M.K. Yu, W.Q. Huang, X. Sun, Y.W. Chung, X. Jiang, Y. Sohma, H.C. Chan, Glucose-induced electrical activities and insulin secretion in pancreatic islet β-cells are modulated by CFTR, Nat. Commun. 5 (2014) 4420.

[47] E.J. Reverri, B.M. Morrissey, C.E. Cross, F.M. Steinberg, Inflammation, oxidative stress, and cardiovascular disease risk factors in adults with cystic fibrosis, Free Radic. Biol. Med. 76 (2014) 261–277.

[48] S. Carrabino, D. Carpani, A. Livraghi, M. Di Cicco, D. Costantini, E. Copreni, C. Colombo, M. Conese, Dysregulated interleukin-8 secretion and NF-kappaB activity in human cystic fibrosis nasal epithelial cells, J. Cyst. Fibros. 5 (2006) 113–119.

[49] J.B. Richman-Eisenstat, P.G. Jorens, C.A. Hébert, I. Ueki, J.A. Nadel, Interleukin-8: an important chemoattractant in sputum of patients with chronic inflammatory airway diseases, Am. J. Phys. 264 (1993) L413–418.